Journal of Crystal Growth 605 (2023) 127071

Contents lists available at ScienceDirect

Journal of Crystal Growth

journal homepage: www.elsevier.com/locate/jcrysgro

Interband transitions of InAs/AlAs Short-Period superlattices grown by molecular beam epitaxy

Lu Yao [a], Wenyang Wang [a], Jinshan Yao [b], Kechao Lu [c], Hong Lu [b,d,*], Changcheng Zheng [c,*], Baile Chen [a,e,*]

[a] School of Information Science and Technology, ShanghaiTech University, Shanghai 201210, P. R. China
[b] National Laboratory of Solid State Microstructures & Department of Materials Science and Engineering, College of Engineering and Applied Sciences, Nanjing University, Nanjing 210093, P. R. China
[c] Division of Natural and Applied Sciences, Duke Kunshan University, Kunshan 215316, P. R. China
[d] Jiangsu Key Laboratory of Artificial Functional Materials, Nanjing University, Nanjing, 210093, P. R. China
[e] Shanghai Engineering Research Center of Energy Efficient and Custom AI IC, Shanghai 201210, P. R. China

ARTICLE INFO

Communicated by Hajime Asahi

Keywords:
A1. Spectroscopic Ellipsometry
A3. Molecular beam epitaxy
A3. Short-period superlattice
B1. Indium aluminum arsenic
B1. Alloys
B2. Semiconducting ternary materials

ABSTRACT

In this work, we use spectroscopic ellipsometry (SE) to study the optical properties of $(InAs)_n/(AlAs)_n$ short-period superlattices (SPS) with different period thicknesses for a wide wavelength range of 250 nm – 1650 nm (about 0.75 eV – 5 eV). Additionally, the $(InAs)_2/(AlAs)_2$ samples grown at various temperatures (450, 475, 500, 525, 550 ℃) were investigated. We extract the dielectric functions and adapt Adachi's model to obtain the interband transition energies of E_0, $E_0+\Delta_0$, E_1, $E_1+\Delta_1$ and E_2. The quantum confinement effect and the strain effect lead to the decrease of E_0, $E_0+\Delta_0$, E_1, $E_1+\Delta_1$ with the increase of period thickness. It is also found that as the growth temperature rises from 450 ℃, all the transition energies decrease as a result of the increase in the amplitude of lateral composition modulation and the relaxation of the compressive strain in InAs layers.

1. Introduction

There is continuous interest in short-period superlattices (SPSs) composed of ultra-thin (a few monolayers) III-V compound semiconductors layers. The optical phonons are confined in superlattices (SLs) by strain [1], which makes SL materials show different band structures and dielectric functions [2]. A unique characteristic of tailoring the electronic and optical properties in superlattices composed of III-V compound semiconductors such as the InAs/AlAs superlattice [3]. The InAs/AlAs SPS on InP substrate has been extensively investigated both optically [4] and electrically [5] recently, due to potential applications in low excess noise Avalanche Photodiodes (APDs) [6]. However, previous studies only focused on the direct bandgap E_0 at Γ point [3–5,7]. In this article, we use spectroscopic ellipsometry (SE) not only to obtain the direct bandgap E_0 and the split off Δ_0 at Γ point, but also the bandgap E_1 as well as the split off Δ_1 at L point, and the bandgap E_2 at X point [8].

There were several reports on E_1, $E_1+\Delta_1$, and E_2 of other kinds of superlattices in the past few years with ellipsometry study. Leibiger *et al.* [9,10] used Adachi's model to extract the E_1 and $E_1+\Delta_1$ transitions of GaAsN/InAs/GaAs superlattices. They found that the blueshift of E_1 can be explained by the effects of biaxial (0 0 1) strain and alloy composition variation. Garriga *et al.* [11] used SE to study the confinement and interlayer coupling effects on the interband transitions of $(GaAs)_n/(AlAs)_n$. It is found that for periods lengths larger than 50 Å, the confinement of the electronic states in the GaAs makes the E_1 and $E_1+\Delta_1$ transitions shift to a higher energy as the period thickness decreases, whereas the effect on E_2 is not apparent. Yoon *et al.* [12] investigated the E_1, $E_1+\Delta_1$, E_0', E_2, $E_2+\Delta_2$, and E_2' of $In_xAl_{1-x}As$ of different composition, where the E_0' and E_2' are the higher transition energies at Γ point and X point, respectively. Lumb *et al.* [13] used Adachi's model to obtain the interband transitions of InAlAs of different doping and fit the extracted E_0 well using the equation of Moss-Burstein shift [14]. Rodriguez *et al.* [15] tested a set of $(InAs)_{15}/(AlAs)_n$ ($n=1$, 2, 5) SLs grown on GaAs substrate to extract E_1 and $E_1+\Delta_1$. It is observed that the transitions shift towards higher energies, and the difference between E_1 and $E_1+\Delta_1$ increased as n increased.

In this work, the interband transitions of $(InAs)_n/(AlAs)_n$ SLs grown

* Corresponding authors.
E-mail address: chenbl@shanghaitech.edu.cn (C. Zheng).

https://doi.org/10.1016/j.jcrysgro.2022.127071
Received 20 October 2022; Received in revised form 5 December 2022; Accepted 26 December 2022
Available online 31 December 2022

on InP substrates by molecular beam epitaxy (MBE) with different monolayers (ML) and different growth temperatures were studied by ellipsometry. We extract the dielectric functions of a series of $(InAs)_n/(AlAs)_n$ SLs samples and use Adachi's model to obtain E_0, $E_0 + \Delta_0$, E_1, $E_1 + \Delta_1$, E_2 transitions. These interband transition energy value of the SLs could be useful for modeling the carrier transport and impact ionization effect in the materials, which has potential applications in avalanche photodiodes design[16]. The effect of strain and growth temperature on interband transitions was investigated. The dielectric functions and the interband transitions of random alloy InAlAs are also extracted to compare with those of Yoon *et al.*[12] and Lumb *et al.*[13], to confirm the reliability of the methods used in this work and the extracted interband transition energies.

2. Experimental details

The structures were grown on semi-insulating InP (0 0 1) substrates by molecular beam epitaxy (MBE), then the substrate was heated to about 530 ℃ to remove the native oxides on InP. A 100 nm-thick $In_{0.52}Al_{0.48}As$ buffer layer was grown at 490 ℃. After growing the buffer layer, the substrate temperature was changed to the desired setpoint to grow the $(InAs)_n/(AlAs)_n$ superlattice layer. There are two groups of $(InAs)_n/(AlAs)_n$ superlattice layers used in the ellipsometric study. One is a series of $(InAs)_n/(AlAs)_n$ (n = 2, 3, 4, 5) superlattice structures grown at the same temperature (450 ℃), and the number of periods is different to keep the same thickness (~255 nm) which is 200 periods $(InAs)_2/(AlAs)_2$, 133 periods $(InAs)_3/(AlAs)_3$, 100 periods $(InAs)_4/(AlAs)_4$, and 80 periods $(InAs)_5/(AlAs)_5$. The other is a series of 200 periods $(InAs)_2/(AlAs)_2$ grown at five different temperatures (450, 475, 500, 525, and 550 ℃). More details about the layer growth procedure can be found in elsewhere [4]. Apart from these two groups of $(InAs)_2/(AlAs)_2$ superlattice samples, an $In_{0.52}Al_{0.48}As$ random alloy (RA) layer was measured as the controlled sample, and the result is used to compare with the interband transition energies of other works to validate our results.

Ellipsometry is a widely used, nondestructive, sensitive characterization technique [17] that can be employed to determine film layer optical constants. It can characterize thin films, surfaces, and microstructure of material by measuring the change in the polarization state of light after reflection. The measured values are expressed as ellipsometric angles psi (Ψ) and delta (Δ). These values are calculated as the ratio ρ of Fresnel reflection coefficients r_p and r_s for p- and s- polarized light, respectively, which can be written in the form

$$\rho = \frac{r_p}{r_s} = tan(\Psi) exp(i\Delta) \tag{1}$$

Since ellipsometry measures the ratio of r_p and r_s, measurements can be highly accurate and reproducible.

In this work, we extracted the optical constants of samples from variable-angle spectroscopic ellipsometry (VASE) using an M−2000UI (J.A. Woollam Co.) with a wide wavelength range of 250 nm − 1650 nm (about 0.75 eV – 5 eV). The SE obtains more sensitivity near Brewster's angle, so all the samples are tested at an angle of incidence of 60°, 65°, 70°, and 75°. The spectroscopic ellipsometry data is analyzed by Complete-EASE 6.50 from J.A. Woolam Co., Inc.

3. Modelling

The SE data analysis process begins by building a layered optical model that corresponds to the realistic structure including roughness and surface oxide layers, so to extract the optical properties of $(InAs)_n/(AlAs)_n$ digital alloy. A multilayer model includes InP-substrate, InAlAs buffer, $(InAs)_n/(AlAs)_n$, and InAs-oxide is employed in this work. The control sample with only InAlAs buffer grown on the InP substrate is also tested to extract dielectric functions of InAlAs random alloy. The $(InAs)_n/(AlAs)_n$ layer is modeled by B-Spline (basis spline) model, which was also previously utilized to fit digital alloy $Al_{0.85}Ga_{0.15}As_{0.56}Sb_{0.44}$ [18]. The B-spline layer model the optical constants using a series of basis-spline functions [19], while the modeled optical constants are Kramers-Kronig (KK) consistent and non-negative to keep the result physically correct. As shown in Fig. 1, the model fits the measured data Ψ and Δ well for different angles. The fit quality is quantified by the Mean-Squared Error (MSE) to show how well the data calculated by the model agrees with the measured SE data [20], which is defined as:

$$MSE = \sqrt{\frac{1}{3n-m}\sum_{i=1}^{n}\left[\left(\frac{\Psi_i^{(m)} - \Psi_i^{(e)}}{\sigma_{\Psi,i}^{(e)}}\right)^2 + \left(\frac{\Delta_i^{(m)} - \Delta_i^{(e)}}{\sigma_{\Delta,i}^{(e)}}\right)^2\right]} \tag{2}$$

where n is the number of points, m is the number of fit parameters, $\sigma_{\Psi,i}^{(e)}$ and $\sigma_{\Delta,i}^{(e)}$ are the standard deviations in data Ψ and Δ, respectively. The superscripts *(m)* and *(e)* indicate the model and experiment data, respectively. The data is fitted using a built-in Levenberg-Marquardt algorithm to find the minimum MSE. The acceptable MSE value depends on the thickness and complexity of the film, so there is no limit to an ideal MSE value, while a lower MSE indicates a better fit. In our work, the MSE values of all samples are smaller than 1.

The extracted real ε_1 and imaginary ε_2 parts of the dielectric function of the $(InAs)_2/(AlAs)_2$ digital alloy layer is shown in Fig. 2. To obtain the interband transition energies in the layer, we employed Adachi's model of the dielectric function to fit the extracted dielectric function, which is shown as the solid line in Fig. 2. The model is the sum of the contributions from each critical point (CP) correspond to E_0, $E_0 + \Delta_0$, E_1, $E_1 + \Delta_1$, E_2 transitions, where E_0, E_1, E_2 are the band gap at Γ point, L point and X point respectively and Δ_0, Δ_1 are the split off. The formulas are briefly presented in the following content.

A. E_0 and $E_0 + \Delta_0$ Transitions.

The contribution of E_0 and $E_0 + \Delta_0$ transitions is given by:

$$\varepsilon^{(0)}(E) = AE_0^{-1.5}\left[f(\chi_0) + \frac{1}{2}\left(\frac{E_0}{E_0+\Delta_0}\right)^{1.5} f(\chi_{so})\right] \tag{3}$$

where

$$f(\chi_0) = \chi_0^{-2}\left[2 - (1+\chi_0)^{0.5} - (1-\chi_0)^{0.5}\right] \tag{4}$$

$$f(\chi_{so}) = \chi_{so}^{-2}\left[2 - (1+\chi_{so})^{0.5} - (1-\chi_{so})^{0.5}\right] \tag{5}$$

$$\chi_0 = \frac{E + i\Gamma_0}{E_0} \tag{6}$$

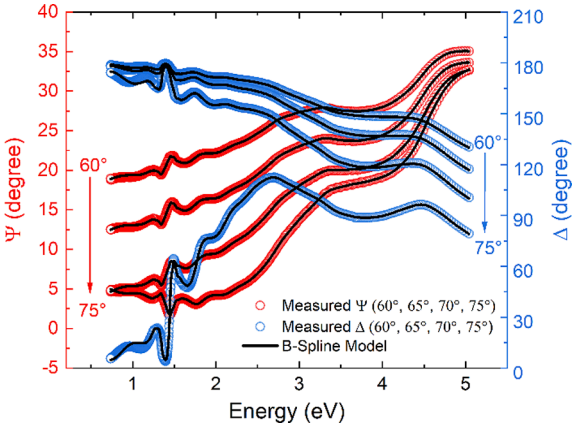

Fig. 1. Measurement of ellipsometric angles Ψ and Δ versus photon energy of $(InAs)_2/(AlAs)_2$ grown at 450 ℃.

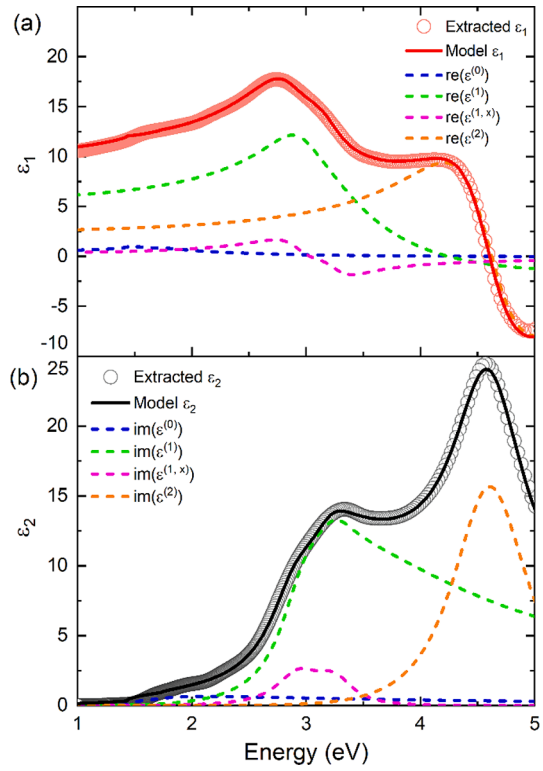

Fig. 2. Fitted result of Adachi's model to the extracted (a)ε_1 and (b)ε_2 of $(InAs)_2/(AlAs)_2$ grown at 450 ℃ and contributions of each transition.

$$\chi_{so} = \frac{E + i\Gamma_0}{E_0 + \Delta_0} \tag{7}$$

and A, Γ_0, are the amplitude and damping constant of E_0 and $E_0 + \Delta_0$ transitions, respectively.

B. E_1 and $E_1 + \Delta_1$ Transition.

The contribution of E_1 and $E_1 + \Delta_1$ transitions is given by:

$$\varepsilon^{(1)}(E) = -B_1\chi_1^{-2}ln\left(1-\chi_1^{2}\right) - B_{1s}\chi_{1s}^{-2}ln\left(1-\chi_{1s}^{2}\right) \tag{8}$$

with

$$\chi_1 = \frac{E + i\Gamma_1}{E_1} \tag{9}$$

$$\chi_{1s} = \frac{E + i\Gamma_1}{E_1 + \Delta_1} \tag{10}$$

where B_1 and B_{1s} are the amplitude, and Γ_1 is the damping constant of E_1 and $E_1 + \Delta_1$ transition.

Additionally, there exists a series of 2D Wannier-type excitons at E_1 CP structure in Adachi's model, which can be approximated to a Lorentzian lineshape:

$$\varepsilon^{(1,x)}(E) = \frac{B_x}{E_1 - E - i\Gamma_1} + \frac{B_{s,x}}{E_1 + \Delta_1 - E - i\Gamma_1} \tag{11}$$

where B_x, $B_{s,x}$ are the amplitude of the ground-state excitonic contribution.

C. E_2 Transition.

The contribution of E_2 transition is given by:

$$\varepsilon^{(2)}(E) = \frac{CE_2^{2}}{E_2^{2} + E^{2} - iE\Gamma_2} \tag{12}$$

where C, Γ_2 are respectively amplitude and damping constant of E_2 transition.

D. Energy Dependent Damping Constant.Γ

The Adachi's model is shown to have extended absorption tails for Lorentzian-broadened E_1, $E_1 + \Delta_1$ and E_2 transitions at low energy regions, which will cause unphysical E_0 value. To solve the problem, Kim *et al.* [21] substituted the damping constant Γ into:

$$\Gamma_i^{'}(E) = \Gamma_i exp[-\alpha_i(\frac{E - E_i}{\Gamma_i})^2] \tag{13}$$

when $\alpha_i = 0$, it is purely Lorentzian broadening, and variation of α_i will change the line shape into a more Gaussian case.

E. The Dielectric Function.

As mentioned above, Adachi's model is the sum of all the cases shown in equations (2), (7), (10), (11), as depicted in Fig. 2, so the dielectric function becomes:

$$\varepsilon(E) = \varepsilon^{(0)}(E) + \varepsilon^{(1)}(E) + \varepsilon^{(1,x)}(E) + \varepsilon^{(2)}(E) \tag{14}$$

4. Results and discussion

We applied the same method described in the previous sections to extract the interband transition energies of InAlAs random alloy and compared with the work of Yoon *et al.*[12] and Lumb *et al.*[13] in Table 1. The sample of Lumb *et al.* is $8.8 \times 10^{15}\,cm^{-3}$ Si-doped $In_{0.52}Al_{0.48}As$. All the transition energies obtained in this work are close to the value shown in reference [12,13], so the reliability of the extracted interband transition energies is confirmed.

We then show the tendencies of optical transition energies as the period thickness varies from $(InAs)_2/(AlAs)_2$ to $(InAs)_5/(AlAs)_5$ monolayers measured by SE at 300 K in Fig. 3. The dotted lines are guides to represent the dependence on the number of monolayers. The values of the transition energies for $(InAs)_n/(AlAs)_n$ (n = 2, 3, 4, 5) are summarized in Table 2. For possible applications to design devices, we presented the best-fit parameters of the linear fitness $E(n) = an + b$ for the extracted interband transitions in Table 3, where n is the number of monolayers, while it does not necessarily mean there is a linear relationship between the number of monolayers and the transition energies.

We observe that, the energies of the optical transitions E_0, $E_0 + \Delta_0$, E_1, $E_1 + \Delta_1$ decrease as the period thickness increases, while there is no obvious change in those of the E_2 transition. Similar results were seen in $(AlAs)_n/(GaAs)_n$ SLs grown along the [001] direction [11]. It can be explained by the effects of quantum confinement of the electronic states in the superlattice [15]. For E_0 and $E_0 + \Delta_0$ transitions, the decreases are larger than those of E_1 and $E_1 + \Delta_1$, because the difference between the energy of the transitions in InAs and AlAs is relatively large, and the effective masses of electrons and holes at Γ point are smaller [15]. Another reason why the change of E_2 is the smallest is that the energies of E_2 transitions for InAs and AlAs are close to each other ($E_{2,InAs}$ = 4.70eV, $E_{2,AlAs}$ = 4.85eV)[22]. In addition, the E_0 characterized by SE is slightly larger than the results of photoluminescence (PL)[4]. The reason may be that PL shows the smallest radiative transition (probably from bounded states below the band edge), which is not completely the same as the direct transition at Γ point [11], and there may be laser-induced heating for PL causing bandgap shrinkage.

In addition to the quantum confinement effects, the strain also influences the optical transitions in $(InAs)_n/(AlAs)_n$ SLs, since there is a large lattice mismatch between InAs and AlAs (a_{InAs}: 6.058 Å, a_{AlAs}: 5.661 Å)[22]. In these structures, the InAs layers are under the in-plane biaxial compressive strain, and the AlAs layers are under the in-plane

Table 1
The interband transitions of $In_{0.52}Al_{0.48}As$ extracted from Adachi's model comparing with data from other references.

Samples	E_0(eV)	$E_0 + \Delta_0$(eV)	E_1(eV)	$E_1 + \Delta_1$(eV)	E_2(eV)
$In_{0.52}Al_{0.48}As$	1.48	1.78	2.98	3.25	4.59
$In_{0.52}Al_{0.48}As$[12]	1.50	1.82	3.06	3.28	4.61
$In_{0.52}Al_{0.48}As$[13]	1.45	1.75	2.93	3.23	4.675

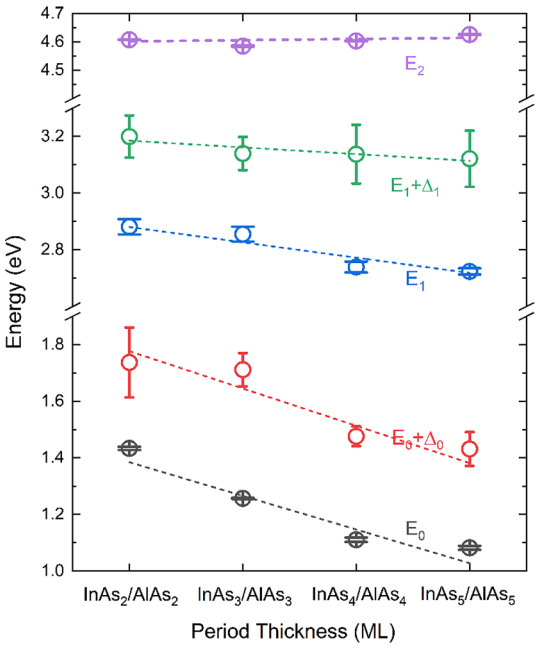

Fig. 3. The interband transitions energies of $(InAs)_n/(AlAs)_n$ (n = 2, 3, 4, 5) verse n. The lines are guides to show the prevailing direction of the data.

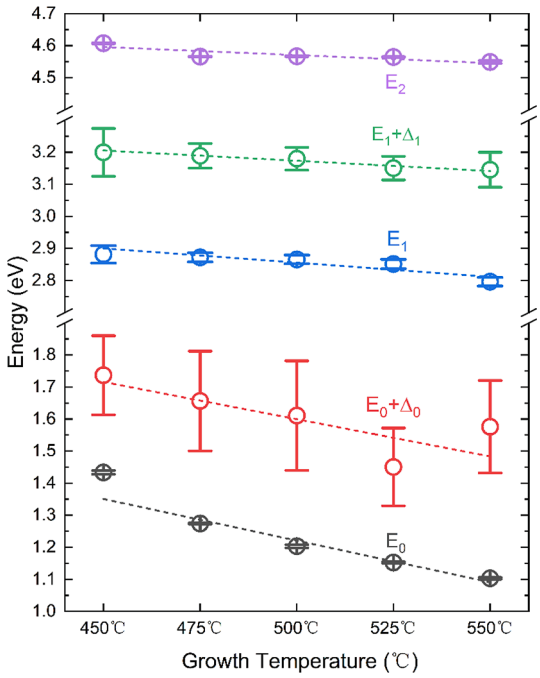

Fig. 4. The interband transitions energies of $(InAs)_2/(AlAs)_2$ grown at different temperatures. The lines are guides to show the prevailing direction of the data.

Table 2
The interband transitions of $(InAs)_n/(AlAs)_n$ (n = 2, 3, 4, 5) extracted from Adachi's model.

Sample	PL data (eV) [4]	E_0(eV)	$E_0 + \Delta_0$(eV)	E_1(eV)	$E_1 + \Delta_1$(eV)	E_2(eV)
$(InAs)_2/(AlAs)_2$	1.41	1.43	1.74	2.88	3.20	4.61
$(InAs)_3/(AlAs)_3$	1.23	1.27	1.71	2.86	3.14	4.58
$(InAs)_4/(AlAs)_4$	1.07	1.11	1.47	2.74	3.14	4.60
$(InAs)_5/(AlAs)_5$	1.01	1.08	1.43	2.72	3.12	4.63

Table 3
Values of the parameters obtrained by fitting the extracted interband transitions to E(n) = an + b.

CP (eV)	a	B
E_0	−0.120	1.641
$E_0 + \Delta_0$	−0.115	1.992
E_1	−0.059	3.007
$E_1 + \Delta_1$	−0.024	3.233
E_2	0.007	4.58

Table 4
The interband transitions of $(InAs)_2/(AlAs)_2$ grown at different temperature extracted From Adachi's model.

Temperature	E_0(eV)	$E_0 + \Delta_0$(eV)	E_1(eV)	$E_1 + \Delta_1$(eV)	E_2(eV)
450℃	1.43	1.74	2.88	3.20	4.61
475℃	1.27	1.66	2.87	3.14	4.57
500℃	1.20	1.61	2.86	3.14	4.56
525℃	1.15	1.45	2.85	3.12	4.56
550℃	1.10	1.58	2.80	3.12	4.55

Table 5
Values of the parameters obtrained by fitting the extracted interband transitions to E(T) = aT + b.

CP (eV)	a	b
E_0	−0.00313	2.798
$E_0 + \Delta_0$	−0.00232	2.761
E_1	−0.00089	3.301
$E_1 + \Delta_1$	−0.00064	3.494
E_2	−0.00050	4.822

biaxial tensile strain as indicated by the Raman measurements (results not shown here). As pointed out by Herzinger *et al.*[23], the E_1 and $E_1 + \Delta_1$ of AlAs decreases under biaxial tensile strain, and the E_1, $E_1 + \Delta_1$ of InAs increase under biaxial tensile strain. According to the work of Wagner *et al.*[24], the E_1 and $E_1 + \Delta_1$ of InAs vary with the relative mismatch, which could be another reason for the increments in the Δ_1 shown in Fig. 3.

Moreover, we show the tendencies of optical transition energies of $(InAs)_2/(AlAs)_2$ as the growth temperature varies from 450 to 550 ℃ in the step of 25 ℃ measured by SE at 300 K in Fig. 4. The values are shown in Table 4. For possible applications to design devices, we presented the best-fit parameters of the linear fitness $E(T) = aT + b$ for the extracted interband transitions in Table 5, where T is the growth temperature of $(AlAs)_2/(GaAs)_2$ SLs, while it does not necessarily mean there is a linear relationship between the growth temperature and the transition energies.

The E_0, $E_0 + \Delta_0$, E_1, $E_1 + \Delta_1$ and E_2 transitions decrease as the growth temperature increases, as depicted in Fig. 4. These shifts may be due to the lateral composition modulation (LCM), which often exists in lattice-mismatched short-period SLs[25]. The lateral composition modulation was also found in InAs/AlAs SPS grown on InP (001) by Millunchick *et al.*[26] and Dorin *et al.*[27]. The amplitude of composition modulation arises from the morphological and compositional instabilities at the surface, which is influenced by the growth temperature. Zhang *et al.*[28] indicated that an increase in lateral composition modulation could lead to a bandgap reduction in InAs/AlAs SPS. As the growth temperature increases, the modulated In-rich regions are enhanced due to the improving In adatom migration, and the In-rich region leads to a lower band-edge energy[28]. Additionally, the Raman measurements shows the compressive strain of InAs layer relaxed as the growth temperature increases, but tensile strain of AlAs is not impacted (results not shown here). The interband transitions energies of InAs layers then decrease as

pointed out by Herzinger *et al.* [23], while those of AlAs layers almost remain no change. As a result, the bandgap reduction of $(InAs)_2/(AlAs)_2$ with the growth temperature in this work can be related to the lateral composition modulation and the relaxation of the compressive strain in InAs layers. As for the application in the optoelectronic devices based on $(InAs)_2/(AlAs)_2$ SPS, the growth temperature of the $(InAs)_2/(AlAs)_2$ SPS should therefore be lower than 450℃ for better uniformity and periodicity with no composition modulation.

5. Conclusion

In summary, we investigated the dependence of the transition energies E_0, $E_0+\Delta_0$ E_1, $E_1+\Delta_1$, E_2, in $(InAs)_n/(AlAs)_n$ digital alloy with different period thicknesses. It has been found that as the period thickness increases, all the transition energies except E_2 decreases with the strain while no obvious change occurs for E_2, which is due to and quantum confinement effect. While as the growth temperature rises from 450 to 550 ℃, all the transition energies, including E_2, decreases in $(InAs)_2/(AlAs)_2$ SPS. The phenomenon can be attributed to the strengthened lateral composition modulation and the relaxation of compressive strain in InAs layer as growth temperature increases. The findings of this work will provide helpful information for further insights into the SPS band structures and instruct the design of optoelectronic devices based on these InAs/AlAs SPS.

CRediT authorship contribution statement

Lu Yao: Formal analysis, Investigation, Methodology, Writing – original draft. **Wenyang Wang:** Investigation, Methodology, Writing – review & editing. **Jinshan Yao:** Investigation, Methodology, Writing – review & editing. **Kechao Lu:** Writing – review & editing. **Hong Lu:** Investigation, Methodology, Writing – review & editing, Supervision, Funding acquisition. **Changcheng Zheng:** Formal analysis, Investigation, Methodology, Writing – review & editing. **Baile Chen:** Formal analysis, Investigation, Methodology, Writing – review & editing, Supervision, Funding acquisition.

Declaration of Competing Interest

The authors declare that they have no known competing financial interests or personal relationships that could have appeared to influence the work reported in this paper.

Data availability

Data will be made available on request.

Acknowledgement

This work was supported in part by the National Key Research and Development Program of China under Grant 2018YFB2201000 and in part by the National Natural Science Foundation of China under Grant 61975121. It was also sponsored by Double First-Class Initiative Fund of ShanghaiTech University. We are grateful to the device fabrication support from the Shanghaitech University Quantum Device Lab.

References

[1] S. Adachi, GaAs and related materials : bulk semiconducting and superlattice properties, World Scientific, Singapore; River Edge, New Jersey, 1994.
[2] D.K. Ferry, J.R. Barker, C. Jacoboni, North atlantic treaty organization, Granular nanoelectronics, Plenum Press, New York, Scientific Affairs Division., 1991.
[3] M. Vazquez, J.P. Silveira, L. Gonzalez, M. Perez, G. Armelles, J.L. Demiguel, F. Briones, Atomic layer molecular-beam epitaxy of inas/alas heterostructures, J. Cryst. Growth 102 (1990) 891–898, https://doi.org/10.1016/0022-0248(90)90857-H.
[4] J.S. Yao, R. Pan, W.Y. Wang, C. Li, B.L. Chen, H. Lu, Y.F. Chen, Large tunable bandgaps in the InAs/AlAs strain-compensated short-period superlattices grown by molecular beam epitaxy, Appl. Phys. Lett. 118 (2021), 252103, https://doi.org/10.1063/5.0054850.
[5] A.K. Rockwell, M. Ren, M. Woodson, A.H. Jones, S.D. March, Y. Tan, Y. Yuan, Y. Sun, R. Hool, S.J. Maddox, M.L. Lee, A.W. Ghosh, J.C. Campbell, S.R. Bank, Toward deterministic construction of low noise avalanche photodetector materials, Appl. Phys. Lett. 113 (2018), 102106, https://doi.org/10.1063/1.5040592.
[6] J. Zheng, Y. Tan, Y. Yuan, A.W. Ghosh, J.C. Campbell, Tuning of energy dispersion properties in InAlAs digital alloys, J. Appl. Phys. 125 (2019), 245702, https://doi.org/10.1063/1.5091694.
[7] Y. Yuan, J.Y. Zheng, Y.H. Tan, Y.W. Peng, A.K. Rockwell, S.R. Bank, A. Ghosh, J. C. Campbell, Temperature dependence of the ionization coefficients of InAlAs and AlGaAs digital alloys, Photonics Res. 6 (2018) 794–799, https://doi.org/10.1364/Prj.6.000794.
[8] S. Adachi, Handbook on physical properties of semiconductors, Kluwer Academic Publishers, Boston, 2004.
[9] G. Leibiger, V. Gottschalch, B. Rheinlander, J. Sik, M. Schubert, Model dielectric function spectra of GaAsN for far-infrared and near-infrared to ultraviolet wavelengths, J. Appl. Phys. 89 (2001) 4927–4938, https://doi.org/10.1063/1.1359422.
[10] G, Leibiger, V, Gottschalch, A, Kasik, B, Rheinlander, J, Sik, M, Schubert, Optical constants, critical points, free carrier effects, and phonon modes of GaAsN single layers and GaAsN/InAs/GaAs superlattices, 2000 IEEE International Symposium on Compound SemiconductorssProceedings of the IEEE Twenty-Seventh International Symposium on Compound Semiconductors (Cat. No. 00TH8498), (2000) 7-12. https://doi.org/10.1109/Iscs.2000.947120.
[11] M. Garriga, M. Cardona, N.E. Christensen, P. Lautenschlager, T. Isu, K. Ploog, Interband transitions of thin-layer GaAs/AlAs superlattices, Phys. Rev. B Condens. Matter 36 (1987) 3254–3258, https://doi.org/10.1103/physrevb.36.3254.
[12] J.J. Yoon, T.H. Ghong, J.S. Byun, Y.D. Kim, D.E. Aspnes, H.J. Kim, Y.C. Chang, J. D. Song, Optical properties of InxAl1−xAs alloy films, Appl. Phys. Lett. 92 (2008), 151907, https://doi.org/10.1063/1.2909546.
[13] M.P. Lumb, M.K. Yakes, M. Gonzalez, J.G. Tischler, R.J. Walters, Optical properties of Si-doped and Be-doped InAlAs lattice-matched to InP grown by molecular beam epitaxy, J. Appl. Phys. 114 (2013), 103504, https://doi.org/10.1063/1.4820519.
[14] G.W. Charache, D.M. DePoy, J.E. Raynolds, P.F. Baldasaro, K.E. Miyano, T. Holden, F.H. Pollak, P.R. Sharps, M.L. Timmons, C.B. Geller, W. Mannstadt, R. Asahi, A. J. Freeman, W. Wolf, Moss-Burstein and plasma reflection characteristics of heavily doped n-type InxGa1-xAs and InPyAs1-y, J. Appl. Phys. 86 (1999) 452–458, https://doi.org/10.1063/1.370751.
[15] J.M. Rodrguez, G. Armelles, J.P. Silveira, M. Vazquez, F. Briones, Optical properties of InAs/AlAs strained-layer superlattices, Phys. Rev. B Condens. Matter 40 (1989) 8570–8572, https://doi.org/10.1103/physrevb.40.8570.
[16] W. Wang, J. Yao, J. Wang, Z. Deng, Z. Xie, J. Huang, H. Lu, B. Chen, Characteristics of thin InAlAs digital alloy avalanche photodiodes, Opt. Lett. 46 (2021) 3841–3844, https://doi.org/10.1364/OL.435025.
[17] H, Fujiwara, Spectroscopic Ellipsometry: Principles and Applications, in: Spectroscopic Ellipsometry, John Wiley & Sons, 2007.
[18] B, Guo, A.H, Jones, S, Lee, S.H, Kodati, B, Liang, X, Xue, N.A, Pfiester, M, Schwartz, M, Winslow, C.H, Grein, T.J, Ronningen, S, Krishna, J.C, Campbell, Optical constants of Al0.85Ga0.15As0.56Sb0.44 and Al0.79In0.21As0.74Sb0.26, Appl Phys Lett, 119 2021 171109. 10.1063/5.0062035.
[19] B. Johs, J.S. Hale, Dielectric function representation by B-splines, Phys. Status Solidi A 205 (2008) 715–719, https://doi.org/10.1002/pssa.200777754.
[20] J. Woollam, CompleteEASE data analysis manual, JA Woollam Co., Inc, United States of America, New England, 2011.
[21] C.C. Kim, J.W. Garland, P.M. Raccah, Modeling the optical dielectric function of the alloy system AlxGa1-xAs, Phys. Rev. B Condens. Matter 47 (1993) 1876–1888, https://doi.org/10.1103/physrevb.47.1876.
[22] S. Adachi, Properties of semiconductor alloys : group-IV, III-V and II-VI semiconductors, Wiley, Chichester, U.K., 2009.
[23] C.M. Herzinger, P.G. Snyder, F.G. Celli, Y.C. Kao, D. Chow, B. Johs, J.A. Woollam, Studies of thin strained InAs, AlAs, and AlSb layers by spectroscopic ellipsometry, J. Appl. Phys. 79 (1996) 2663–2674, https://doi.org/10.1063/1.361137.
[24] J. Wagner, J. Schmitz, N. Herres, G. Trankle, P. Koidl, Study of composition and critical-point broadening in InAs/Ga1-xInxSb superlattices using spectroscopic ellipsometry, Appl. Phys. Lett. 70 (1997) 1456–1458, https://doi.org/10.1063/1.118560.
[25] A. Zunger, S. Mahajan, Handbook on semiconductors, Atomic ordering and phase separation in III–V alloy semiconductors, North-Holland, Amsterdam, 1994, p. 1399.
[26] J.M. Millunchick, R.D. Twesten, D.M. Follstaedt, S.R. Lee, E.D. Jones, Y. Zhang, S. P. Ahrenkiel, A. Mascarenhas, Lateral composition modulation in AlAs/InAs short period superlattices grown on InP(001), Appl. Phys. Lett. 70 (1997) 1402–1404, https://doi.org/10.1063/1.118589.
[27] C. Dorin, J.M. Millunchick, Lateral composition modulation in AlAs/InAs and GaAs/InAs short period superlattices structures: the role of surface segregation, J. Appl. Phys. 91 (2002) 237–244, https://doi.org/10.1063/1.1421240.
[28] Y. Zhang, A. Mascarenhas, Electronic and optical properties of laterally composition-modulated AlxIn1-xAs, GaxIn1-xP, and GaxIn1-xAs alloys, Phys. Rev. B 57 (1998) 12245–12254, https://doi.org/10.1103/PhysRevB.57.12245.